JOURNAL OF Applied Polymer SCIENCE

Enhanced thermoelectric performance by alcoholic solvents effects in highly conductive benzenesulfonate-doped poly(3,4-ethylenedioxythiophene)/graphene composites

Hyun Ju, Myeongjin Kim, Jooheon Kim
School of Chemical Engineering & Materials Science, Chung-Ang University, Seoul 156-756, Republic of Korea
Correspondence to: J. Kim (E-mail: jooheonkim@cau.ac.kr)

ABSTRACT: Benzenesulfonate-doped poly(3,4-ethylenedioxythiophene) (PEDOT-Bzs)/graphene thermoelectric (TE) composites with various graphene filler contents were synthesized in five different kinds of solvents. Dodecylbenzenesulfonic acid (DBSA) was used to achieve good dispersion of graphene into the PEDOT matrix. Among the synthesized PEDOT materials, the one synthesized in methanol (PEDOT-MeOH) had the highest electrical conductivity. X-ray photoelectron spectroscopy (XPS) analysis showed almost the same charge carrier concentration for all PEDOT materials. However, the X-ray diffraction (XRD) analysis highlighted the enhancement of PEDOT chain stacking by shorter-chain alcoholic solvents, as a result of which the carrier mobility and electrical conductivity were increased. The electrical conductivity and the Seebeck coefficient of the PEDOT/graphene composites were significantly improved with increasing the graphene content, which strongly depended on increased carrier mobility. The thermal conductivity of the composites exhibited relatively small changes, attributed to phonon scattering effects. The maximum TE efficiency of the PEDOT-MeOH/graphene composite with 75 wt % graphene showed a substantially improved value of 1.9×10^{-2}, higher than that of the other PEDOT/graphene composites. © 2015 Wiley Periodicals, Inc. J. Appl. Polym. Sci. **2015**, *132*, 42107.

KEYWORDS: composites; conducting polymers; graphene and fullerenes; nanotubes; properties and characterization

Received 4 November 2014; accepted 15 February 2015
DOI: 10.1002/app.42107

INTRODUCTION

Thermoelectric (TE) solid state heating/cooling devices that directly convert thermal to electrical energy and vice versa have great potential for energy harvesting. Previous studies have mainly involved relatively high efficient inorganic TE materials, including semiconductors such as Bi_2Te_3, Bi-Te alloys, $CoSb_3$, SiGe, and MgSi, conducting oxides such as $NaCo_2O_4$ and $CaMnO_3$, and metal alloys such as BiSb.[1–3] However, high cost of the raw materials, potential for heavy metal pollution, and processing difficulties limit widespread practical applications of these materials. In this regard, recent studies have focused on TE composites consisting of an inorganic conductive filler and an organic polymer matrix, which have become promising alternatives to inorganic TE materials.

The dimensionless efficiency of a TE material, ZT, can be calculated as $ZT = (S^2 \cdot \sigma \cdot T)/\kappa$, where S is the Seebeck coefficient, σ is the electrical conductivity, κ is the thermal conductivity, and T is the absolute temperature. In principle, in order to achieve a high ZT, a TE material requires high electrical conductivity, high Seebeck coefficient, and low thermal conductivity. The most important among these properties is the high electrical conductivity. Conductive fillers, such as carbon nanotube (CNT), graphene, and carbon black have been frequently used to enhance the electrical conductivity. Wang *et al.* reported a highly oriented polyaniline (PANI)/CNT composite with a power factor ($S^2 \cdot \sigma$) of 0.18 μW/m K^2.[4] Du *et al.* found a a power factor of 0.96 μW/m K^2 for a dimethyl sulfoxide (DMSO)-doped poly(3,4-ethylenedioxythiophene)poly(styrenesulfonate) (PEDOT : PSS) film filled with a conductive carbon black filler.[5] Wang *et al.* prepared a PANI/graphene nanocomposite film, which achieved a maximum power factor of 19 μW/m K^2.[6] Graphene is the best filler material for achieving high electrical conductivity among the carbon-based materials, because of its sp^2 hybrid carbon atoms and superior charge carrier mobility.

However, in addition to a high electrical conductivity of the filler, a large electrical conductivity of the organic polymer matrix is also required for achieving high TE efficiency. Many studies have thus employed conductive polymers, such as PANI, PEDOT : PSS, and polypyrrole (PPy) as organic polymer matrix. Mateeva *et al.* reported that an acid-doped PANI produced a maximum ZT of 10^{-5} at room temperature.[7] Kim *et al.* prepared a ~1 μm-thick spin-coated PEDOT : PSS film whose

ZT value was found to be 0.002.[8] Wang *et al.* studied a *p*-toluenesulfonic acid (TSA)-doped PPy with a power factor of 0.08 $\mu W/m \cdot K^2$.[9] Moreover, other studies have explored the effect of the interaction between solvent molecules and the conductive polymer chains for further enhancing of the electrical conductivity of the conductive polymer. Nardes *et al.* enhanced the electrical conductivity of PEDOT : PSS thin films by adding high-boiling solvents like sorbitol to the aqueous dispersion.[10] Kim *et al.* obtained a high electrical conductivity (~80 S/cm) of PEDOT : PSS film synthesized with various organic solvents.[11] However, not many studies investigating PEDOT as a TE material, as well as the manipulation of solvent effects on the conductive PEDOT, have been reported to date.

Recently, Kim *et al.* reported that ferric benzenesulfonate ($Fe(Bzs)_3$) is a better oxidant for achieving higher electrical conductivity in the 3,4-ethylenedioxythiophene (EDOT) polymerization process than the generally used oxidant, ferric *para*-methylbenzenesulfonate ($Fe(p\text{-}MeBzs)_3$).[12] Although the enhanced electrical conductivity of benzenesulfonate-doped PEDOT (PEDOT-Bzs) is ~49 S/cm, this value does not meet the requirements of high performance TE materials. Therefore, the effect of the interaction between solvent and PEDOT chains needs to be studied to enhance the electrical conductivity of the PEDOT-Bzs.

In this article, a promising strategy for enhancing the TE properties of filler/conductive polymer composites was provided. TE PEDOT-Bzs/graphene composites were fabricated with various contents of high-electrical conductive graphene. Five types of alcoholic solvents were employed during the EDOT polymerization process to improve the electrical conductivity of the PEDOT matrix. The EDOT monomers were polymerized with $Fe(Bzs)_3$ in methanol (PEDOT-MeOH), ethanol (PEDOT-EtOH), 1-propanol (PEDOT-PpOH), *n*-butanol (PEDOT-BtOH), and 1-hexanol (PEDOT-HxOH) solvents. The alkyl chains of the different alcoholic solvents affected stacking of the PEDOT-Bzs chains and led to different charge carrier mobility and TE performance. Dodecylbenzenesulfonic acid (DBSA) was used to act simultaneously as a surfactant for forming graphene micelles and a doping agent to coat the PEDOT layer on the graphene surface. The individual graphene particles were well distributed because the coated PEDOT layer has a marked affinity for the PEDOT matrix, achieving a high conductivity through the electrically connected filler-matrix network. Several TE properties of the PEDOT/graphene composites were examined, such as electrical conductivity, Seebeck coefficient, thermal conductivity, power factor, and figure of merit.

EXPERIMENTAL SECTION

Materials

The 3,4-ethylenedioxythiophene ($C_6H_6O_2S$, EDOT) monomer (Clevios M) was purchased from Bayer AG. Graphene nanopowder was purchased from Graphene Supermarket. DBSA ($C_{12}H_{25}C_6H_4SO_3H$), ammonium persulfate ($(NH_4)_2S_2O_8$, APS), and various alcoholic solvents, such as methanol (CH_3OH), ethanol (C_2H_5OH), 1-propanol (C_3H_7OH), *n*-butanol (C_4H_9OH), and 1-hexanol ($C_6H_{13}OH$), were purchased from Daejung Chemicals & Metals (Seoul, Korea). Benzene (C_6H_6), sulfuric acid (H_2SO_4), and ferric chloride hexahydrate ($FeCl_3 \cdot 6H_2O$) were purchased from Sigma Aldrich.

Fabrication of PEDOT Nanocoating on Graphene

Graphene powder (0.1 g) and 0.326 g of DBSA ($M_W = 326.5$) were added to 50 mL of deionized (DI) water to prepare the graphene colloidal solution which was stirred at 30°C for 1 h. After that, 0.472 g of EDOT ($M_W = 142.18$) was added to the aqueous micellar dispersion and stirred at 30°C for 1 h. Then, 10 mL of DI water and 1.824 g of ammonium persulfate ($M_W = 228.2$) solution were added to the colloidal solution. This solution was stirred steadily with the temperature maintained at 30°C. After 24 h, the resulting mixture was centrifuged at 8000 rpm for 30 min. Then, the supernatant was poured into a bottle and DI water was added to the sediment. This solution was redispersed via ultra-sonication and mechanical shaking for 1 h. The centrifugation to remove supernatant and the redispersion process were repeated five or more times to increase the purity of the resulting powder. Finally, the resulting product was dried in a vacuum oven at 60°C for 24 h.

Synthesis of $Fe(Bzs)_3$

Sulfuric acid and benzene were reacted in a round-bottom flask at 150°C for 1 h for synthesizing benzenesulfonic acid. The molar ratio between benzene and sulfuric acid was 1 : 1. Then, the product was collected via recrystallization using a rotary evaporator. The obtained benzenesulfonic acid was dried in a vacuum oven at 60°C for 1 h. Afterwards, benzenesulfonic acid and methanol were dispersed in a round-bottomed 3 neck flask. The dissolving water of ferric chloride hexahydrate ($FeCl_3 \cdot 6\ H_2O$) was added dropwise to the solution at 230°C and refluxed for 1 h. The ferric chloride hexahydrate to benzenesulfonic acid mole ratio was 1 : 3. The resulting powder was filtered and refluxed at least five times in an acetonitrile/methanol solvent, after which the filtered product was dried at 60°C for 24 h in a vacuum oven.

Synthesis of PEDOT-Coated PEDOT/Graphene Composites

It was assumed that the graphene particles had no effect on the kinetics of the EDOT polymerization. The overall EDOT polymerization process in the solvent is described in Figure 1. EDOT monomer and $Fe(Bzs)_3$, which acted as both oxidant and initiator, were combined for the chemical polymerization. Prior to beginning the experiment, the $Fe(Bzs)_3$ was dried in a vacuum oven at 80°C for 48 h to remove residual moisture. 7.524 g (16 mmol) of $Fe(Bzs)_3$ with different weight percentages of the PEDOT coated graphene filler (0, 15, 30, 45, 60, 75, and 90 wt %) were dispersed in 300 mL of methanol at 30°C for 1 h. 2.832 g (20 mmol) of EDOT monomer were added to the mixture at 65°C for 1 h for creating the polymer chains. Afterwards, the reaction temperature was increased from 65 to 150°C with vigorous stirring for about 20 min to finish the polymerization. The resulting product was washed with methanol solvent and filtered two or three times to eliminate residual oxidant and EDOT monomer. Finally, the filtered powder was dried in a vacuum oven at 60°C for 24 h. The same procedure was employed to prepare composites with other solvents (ethanol, 1-propanol, *n*-butanol, and 1-hexanol).

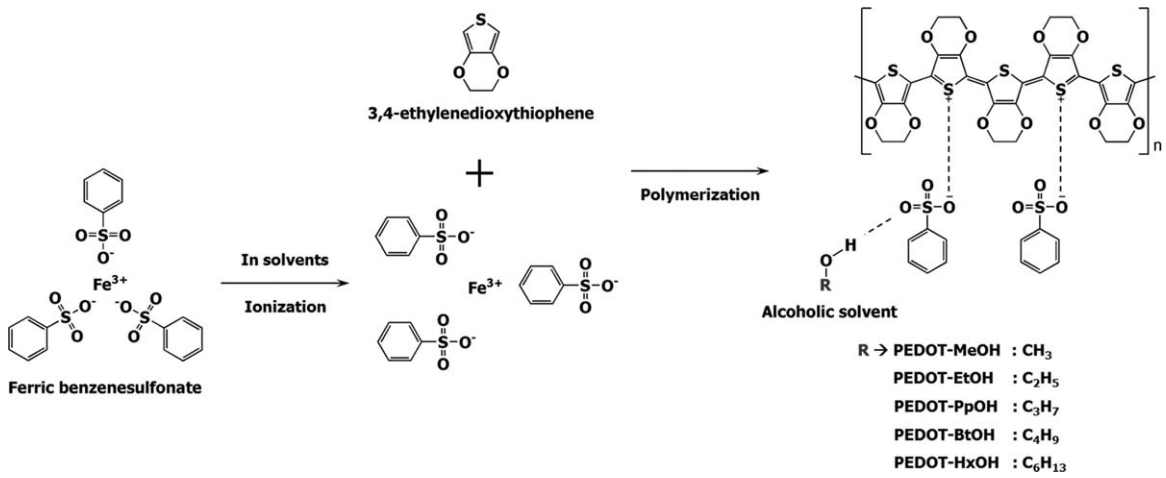

Figure 1. Schematic representation of the EDOT polymerization process in various solvents.

Composite Characterization

Fourier transform infrared (FTIR, Bio-rad FTS-1465) spectra of the composites were obtained using pressed disk-shaped pellets of the samples mixed with potassium bromide (KBr), performing an average of 32 scans in the 500–4000 cm^{-1} radiation region. The doping level of the PEDOT was calculated by X-ray photoelectron spectroscopy (XPS, Thermo U. K. K-alpha) with a monochromated Al Kα X-ray source (1486.6 eV) and a hemispherical analyzer. During curve fitting, the Gaussian peak widths in each spectrum were found to be constant. The morphology and microstructure of the composites were determined by field-emission transmission electron microscopy (FE-TEM, JEM-2100F). The amount of PEDOT coating on the graphene surface was determined by thermogravimetric analysis (TGA, TGA-2050, TA instrument). Samples were heated from 25 to 600°C at a heating rate of 10°C/min under a nitrogen atmosphere and the thermal degradation of the sample was plotted. A four-point probe method with disk-shaped compressed pellets was used to measure the electrical conductivity. The pellets were made using a press machine at room temperature and 50 MPa pressure and their thickness was measured with a digital micrometer. X-ray diffraction (XRD, New D8-Advance/Bruker-AXS) at 40 mA, 40 kV, and a scan rate of 1°/s with a 2θ range of 5°–35° with Cu Kα radiation (0.154056 nm) was used to characterize the orthorhombic structure of PEDOT materials. A homemade device containing a pair of thermocouples and voltmeters was used to measure the Seebeck coefficient, S. The value was determined from the linear relationship between the thermal electromotive force (ΔV) and temperature difference (ΔT) between the two ends of the composite pellets ($S = \Delta V/\Delta T$). The thermal conductivity of the composite was calculated from the relation $\kappa = \alpha \cdot \rho \cdot C_P$ where α is the thermal diffusivity, C_P is the specific heat, and ρ is the bulk density of the material. LFA 447 Nanoflash (NETZSCH) was used to measure the thermal diffusivity. The specific heat was measured using a differential scanning calorimetry system (DSC 131 evo, Setaram Instrumentation). The DSC measurements described the thermal transition behavior of the composites, and the samples were heated from −20 to 120°C at a rate of 10°C/min under a nitrogen atmosphere.

RESULT AND DISCUSSION

PEDOT-Coated Graphene Analysis

FTIR analysis was performed to characterize the structure of the fabricated PEDOT-coated graphene. Figure 2 shows the FTIR spectra of graphene, PEDOT, and PEDOT-coated graphene filler. A large peak at about 3400 cm^{-1} from all samples denotes the O—H vibrations of adsorbed surface water. Figure 2(a) shows the typical signals of graphene at 1633 cm^{-1} (aromatic C=C bond), 1734 cm^{-1} (C=O vibrations), and 1052 cm^{-1} (C—O bond stretching).[13–15] The IR spectrum of pure PEDOT prepared by chemical polymerization is shown in Figure 2(b). The peaks at 1068 and 1234 cm^{-1} originate from the C—O stretching band of ethylenedioxy group in the PEDOT structure.[16] The C—S bond stretching of the thiophene rings of the PEDOT produces the peaks at 989, 856, and 700 cm^{-1}. The C—C and C=C bonds of the quinone structure of the

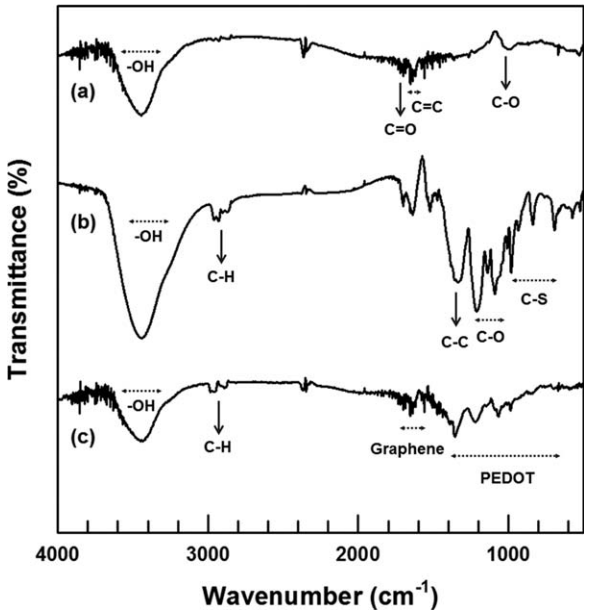

Figure 2. FTIR spectra of (a) raw graphene, (b) pure PEDOT, and (c) PEDOT-coated graphene.

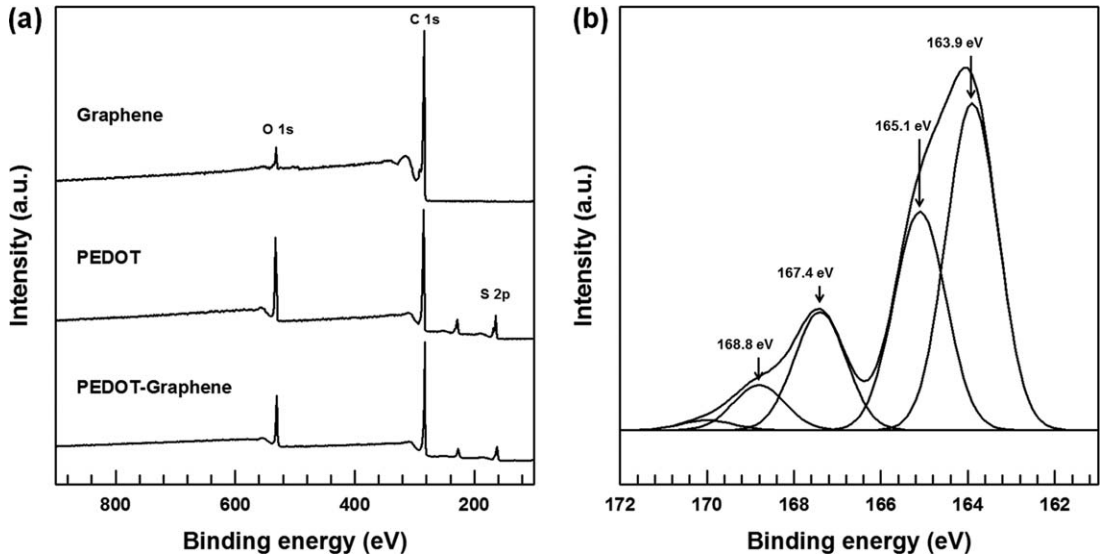

Figure 3. XPS spectra of (a) raw graphene, PEDOT, and PEDOT-coated graphene (wide scan), (b) PEDOT-coated graphene (S 2p core level).

thiophene ring generate a band at ~1357 cm^{-1}.[17] The DBSA was doped into the PEDOT, which exhibited aliphatic C—H bond stretching in the range between 2850 and 3000 cm^{-1}.[18] The spectrum of the synthesized PEDOT-coated graphene filler shown in Figure 2(c) appears to be a combination of peaks from both raw graphene and pure PEDOT.

XPS analysis provided further information about the PEDOT-coated graphene filler. Figure 3(a) shows the XPS survey spectra of graphene, pure PEDOT, and PEDOT-coated graphene. The graphene spectrum was composed of only two elements, C and O, while C, O, and S signals emerged in the pure PEDOT spectrum. The peaks at the C, O, and S positions were also observed in the PEDOT-coated graphene spectrum, but the C/O atomic ratio was higher than that of PEDOT, because graphene mainly consists of carbon atoms. This result implies that the PEDOT-coated graphene filler was successfully synthesized in this polymerization process, as further confirmed by the FE-TEM analysis discussed below.

Furthermore, investigation of the S 2p core-level spectrum was also carried out to estimate the doping level of the PEDOT coating on the graphene surface. The PEDOT coating acted as an electrically connective layer between the PEDOT matrix and graphene. The doping level is directly related to the electrical conductivity, because the positions of the dopant in the conductive polymer chains affect the electron pathways.

S 2p core-level spectra for the DBSA-doped PEDOT on the graphene surface are shown in Figure 3(b). The doping level was calculated from the measured areas via the deconvolutions of the XPS signals, based on the different binding energies of sulfur atoms in the DBSA and PEDOT. Two large peaks in the relatively low binding energy region were observed at both 163.9 and 165.1 eV, indicating sulfur atom spin-splitting in PEDOT. The sulfur atoms in the DBSA ($R\text{-}SO_3$) doped into the PEDOT chain exhibited a binding energy of 167.4 eV.[19] The peak of the sulfur atoms in the oxidized form (SO_3^-) of undoped DBSA appeared at a binding energy of 168.8 eV.[20] The areas corresponding to the $R\text{-}SO_3$ of the DBSA-doped PEDOT, divided by the PEDOT signals, allow a direct estimation of the doping level. On the basis of the measured areas, the DBSA-doped PEDOT layer had a 21.7% doping level.

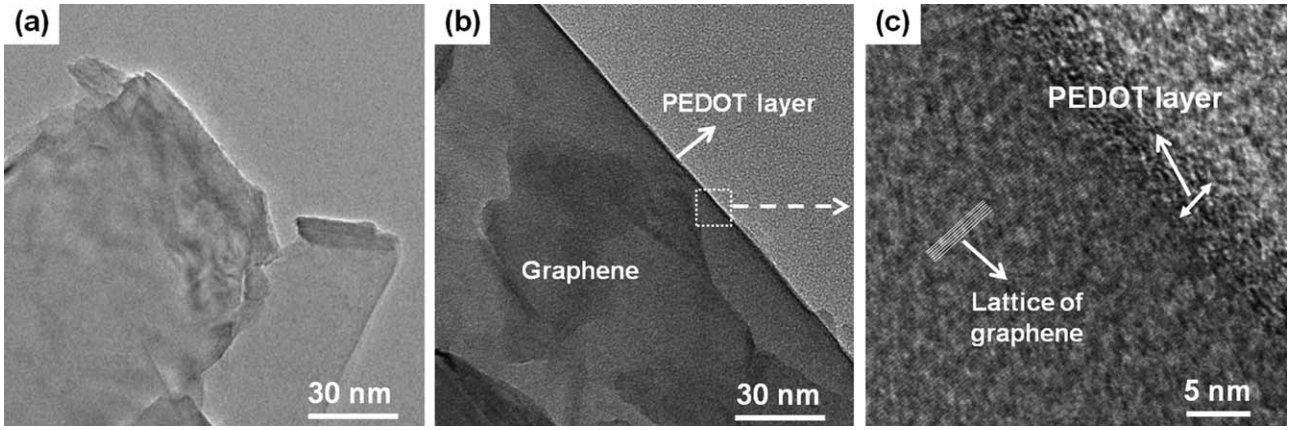

Figure 4. FE-TEM images of (a) raw graphene, (b) PEDOT-coated graphene (low magnification), and (c) PEDOT-coated graphene (high magnification).

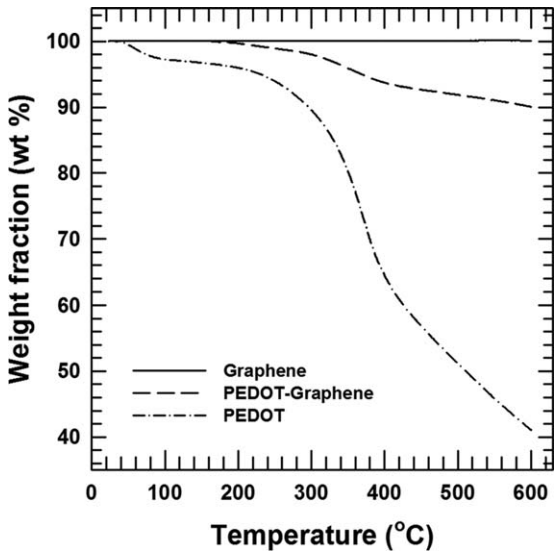

Figure 5. TGA curves of raw graphene, PEDOT-coated graphene, and pure PEDOT.

The TEM analysis directly confirms the successful synthesis of the coated PEDOT layer on the graphene surface. Figure 4(a) shows a TEM image of raw graphene sheet, which is almost transparent and has a very smooth surface. Figure 4(b) presents a low-magnification TEM image of the PEDOT-coated graphene, highlighting the presence of the coating layer on the external graphene surface. The coated PEDOT layer was clearly revealed in the high-magnification TEM image [Figure 4(c)]. It was easy to distinguish the PEDOT from the graphene region due to the distinct lattice pattern of the graphene in the TEM image, despite the fact that the graphene sheet was coated by only a thin nanosized PEDOT layer.

Figure 5 shows the TGA thermograms of raw graphene, pure PEDOT, and PEDOT-coated graphene, which allow us to analyze the level of PEDOT coating more quantitatively. Raw graphene exhibited outstanding thermal stability with no weight loss up to a temperature of 600°C. The weight loss between 50 and 100°C may be due to the moisture absorbed from the PEDOT. The main thermal degradation of the PEDOT was observed at ~300°C in both pure PEDOT and PEDOT-coated graphene samples, whose weights at 600°C were 41.1 and 90.1 wt % of the initial weights, respectively. On the basis of these data, the amount of PEDOT coating on the graphene surface was estimated as 16.8 wt %.

Electrical Conductive Behavior of PEDOT Matrices

Figure 6 shows the electrical conductivity of five types of PEDOT materials with different molar ratio of oxidant. Electrical conductivity increased up to 0.8 molar ratio in equivalent EDOT monomers after which it decreased dramatically for further increases in the oxidant ratio. This effect is due to the increase in undoped oxidants remaining in the PEDOT chains. When the oxidant ratio increases above 0.8, two types of oxidants existed in the EDOT polymerization process: ionic oxidants, such as Fe^{3+} in the solvent and benzenesulfonate anions (Bzs^{-}) doped into the PEDOT main chain, and unionized oxidants that remained in the $Fe(Bzs)_3$ form and thus hampered electrical conduction.[21]

PEDOT-MeOH had the highest electrical conductivity among the PEDOT materials. The electrical conductivity can be expressed in the well-known form:

$$\sigma = n \cdot e \cdot \mu \quad (1)$$

where σ is the electrical conductivity, n is the charge carrier concentration, e is the charge per carrier, and μ is the carrier mobility. Thus, the electrical conductivity is directly connected with changes in charge carrier concentration and mobility.

The effect of charge carrier concentration was relatively investigated to the differences in the doping level of the polymer chains.[12] The oxidants were introduced into the conjugated PEDOT chains and their positions affect the electron pathways. Therefore, higher doping levels of the PEDOT chains could exhibit higher charge carrier concentration. The doping ratio differences of the PEDOT materials were calculated via XPS analysis.

Figure 7 shows the S 2p core level spectra of five kinds of PEDOT materials. The double peaks at 163.9 and 165.1 eV denote the spin-splitting in the sulfur atoms of PEDOT. The binding energy peaks of the doped oxidants in the PEDOT chain were observed at 167.6 eV, while the peaks at 169.1 eV arise from the sulfonic acid group from undoped oxidants.[19] The doping level could be estimated from the ratio of the signals corresponding to doped oxidants and undoped PEDOT. On the basis of these measured areas, the PEDOT-MeOH had molecular doping levels of 32.8%, which was approximately the same level measured for PEDOT-EtOH (32.7%), PEDOT-PpOH (33%), PEDOT-BtOH (32.5%), and PEDOT-HxOH (32.1%). This result means that the change of electrical conductivity is not caused by a different doping level or a different charge carrier concentration.

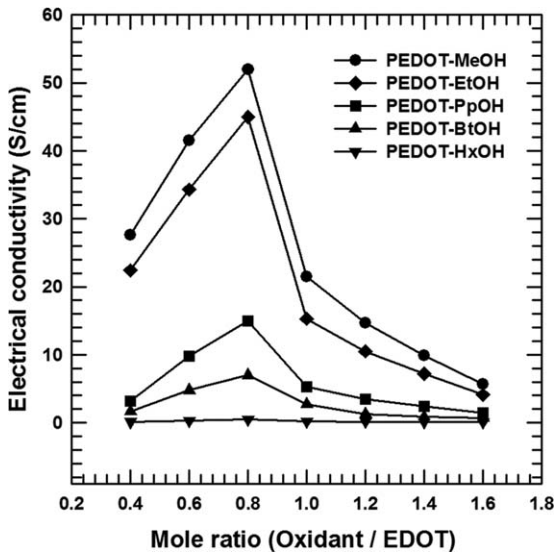

Figure 6. Electrical conductivity of pure PEDOT-MeOH, PEDOT-EtOH, PEDOT-PpOH, PEDOT-BtOH, and PEDOT-HxOH with different mole ratio of the oxidants.

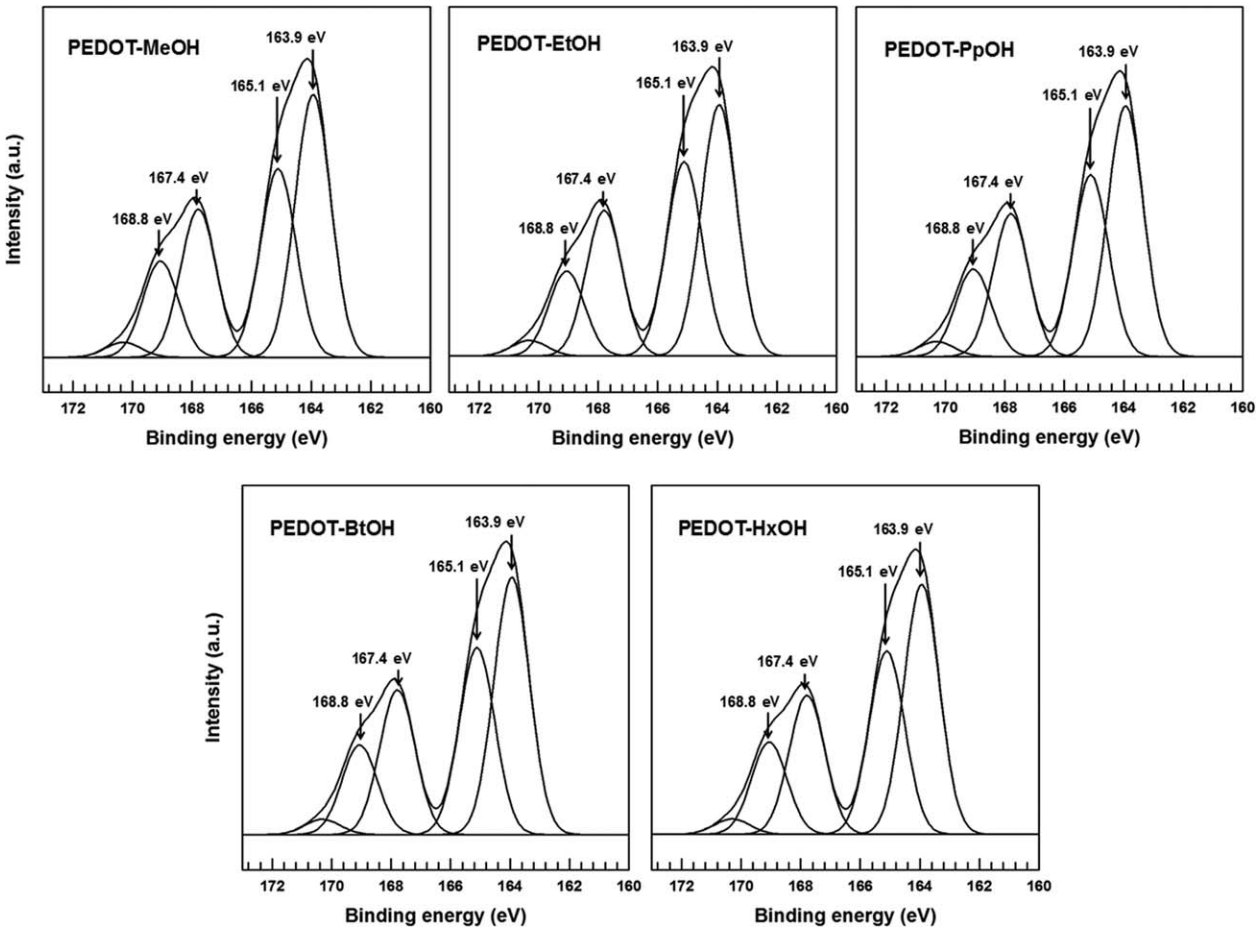

Figure 7. S 2p core level XPS spectra of PEDOT-MeOH, PEDOT-EtOH, PEDOT-PpOH, PEDOT-BtOH, and PEDOT-HxOH.

On the basis of the previous discussion, charge carrier mobility effects could be the only reason for electrical conductivity changes, as a result of structural changes of the PEDOT-Bzs formed in the various solvents. The solvent affects the molecular ordering of the PEDOT chains in the polymerization process; stronger interchain interactions could reduce the charge carrier hopping barrier between PEDOT chains, leading to higher charge carrier mobility and increasing the electrical conductivity.

The XRD analysis provided evidence for the different conductivities induced by the different PEDOT chain structures. Figure 8 shows the XRD patterns of PEDOT-MeOH, PEDOT-EtOH, PEDOT-PpOH, PEDOT-BtOH, and PEDOT-HxOH. As shown in Figure 8, PEDOT-MeOH exhibits pronounced XRD peaks at $2\theta = 6.8°$, 13°, and 26.2°, corresponding to the (1 0 0), (2 0 0), and (0 2 0) planes of orthorhombic PEDOT, respectively. The lattice parameters of the PEDOT-Bzs ($a = 12.99$ Å, $b = 6.8$ Å, $c = 3.4$ Å) were calculated by the Bragg equation:

$$d = \frac{\lambda}{2 \cdot \sin\theta} \tag{2}$$

where λ is the wavelength of the incident wave, d is the spacing between the planes in the atomic lattice, and θ is the angle between the incident ray and the scattering planes. The parameters estimated for PEDOT-MeOH were in agreement with previously reported values, indicating the existence of a PEDOT crystalline phase.[12]

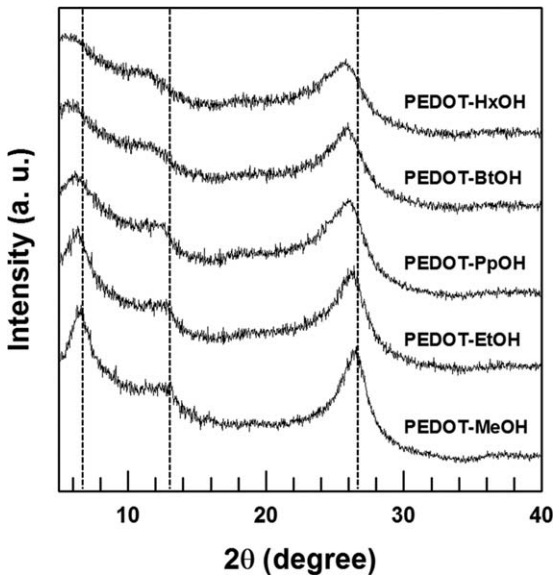

Figure 8. XRD patterns of PEDOT-MeOH, PEDOT-EtOH, PEDOT-PpOH, PEDOT-BtOH, and PEDOT-HxOH.

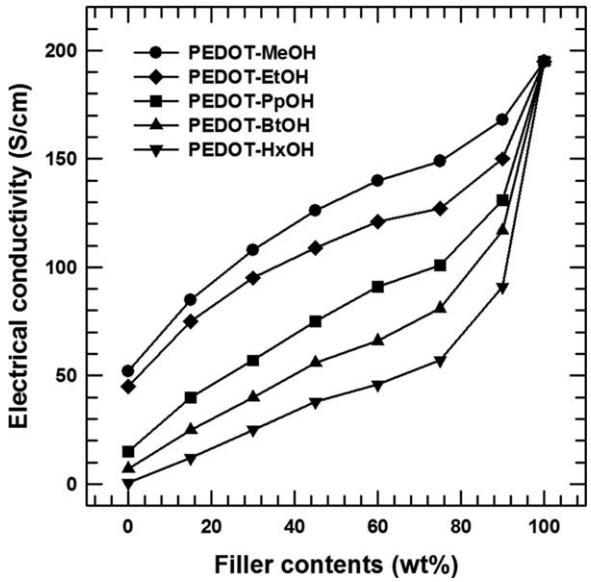

Figure 9. Electrical conductivity of the PEDOT/graphene composites for PEDOT-MeOH, PEDOT-EtOH, PEDOT-PpOH, PEDOT-BtOH, and PEDOT-HxOH.

All peak angles corresponding to the (1 0 0), (2 0 0), and (0 2 0) planes of PEDOT-MeOH were shifted to slightly higher values than those of other PEDOT materials. From the Bragg equation, higher peak angles reflect a decrease in the distance between neighboring polymer chains. In case of the (1 0 0) plane, PEDOT-MeOH had an interchain distance along the *a*-axis within the PEDOT chain stack of 12.99 Å, shorter than other polymerized EDOT materials. The parameter *b* corresponding to the (2 0 0) plane, which represents the distance between polymer chains stacked on top of each other, was calculated as 6.8 Å, which was the shortest value measured for PEDOT materials in this study. The shift of the (0 2 0) reflection plane to a higher value reflects a short intrachain distance (3.4 Å) of the neighboring thiophene rings in the conjugated backbone.

This result was attributed to the participation of the alcoholic solvent in the EDOT polymerization process via the formation of hydrogen bonds between the OH groups of the solvent and sulfonate groups of benzenesulfonate anions, because the hydrogen bond between the alcoholic solvent and the oxygen atoms of PEDOT is very weak.[22]

This structural difference, caused by the shorter chain alcoholic solvent, enhanced the stacking of the PEDOT-Bzs chains. The charge carrier hopping barrier was thus reduced by the decrease of both intra- and interchain stacking distances of the conjugated polymer, and as a result the carrier mobility and electrical conductivity were increased. On the contrary, solvent with longer chains could prevent efficient packing of the PEDOT chains, resulting in increase of the carrier hopping barrier and decrease of the carrier mobility.

Thermoelectric Properties

Figure 9 shows the electrical conductivity of the composites, which is a crucial factor for defining the TE performance of the material. The electrical conductivity of the PEDOT/graphene composites exhibited a clear increase upon addition of graphene filler. The graphene filler can form a strong electrically conductive network with the conjugated PEDOT chains. The graphene has a high intrinsic carrier mobility (200,000 cm^2/V s) and facilitate carrier transfer by means of the π–π interaction with the backbone of the conducting PEDOT, which can greatly reduce the charge carrier hopping barrier, and eventually the charge carrier mobility is increased.[4,23,24] Therefore, as the graphene filler content was increased, a higher electrical conductivity was obtained.

Moreover, the rank order of electrical conductivity, according to the solvent type of the PEDOT matrix, was also determined as PEDOT-MeOH > PEDOT-EtOH > PEDOT-PpOH > PEDOT-BtOH > PEDOT-HxOH. This result is attributable to the difference in polymer chain stacking of the PEDOT matrix induced by the solvent.

As an another key factor, the Seebeck coefficients for the 0, 15, 30, 45, 60, 75, 90, and 100 wt % graphene fillers with the five different PEDOT matrices are shown in Figure 10. The Seebeck coefficient was also markedly improved with the increase of graphene content, and this effect was strongly dependent on the increase of carrier mobility.[25] These dramatic simultaneous improvements of both electrical conductivity and Seebeck coefficient represent an ideal condition for manipulating the TE performance of the material.

Furthermore, Figure 10 illustrates the slight ordering of the Seebeck coefficient measured for the different kinds of polymerized EDOT materials (PEDOT-MeOH > PEDOT-EtOH > PEDOT-PpOH > PEDOT-BtOH > PEDOT-HxOH), which originated from the increase in carrier mobility through the solvent effect.

Figure 11 shows the thermal conductivity of the PEDOT/graphene composites in relation to the graphene content. Compared with the net enhancement of electrical conductivity and

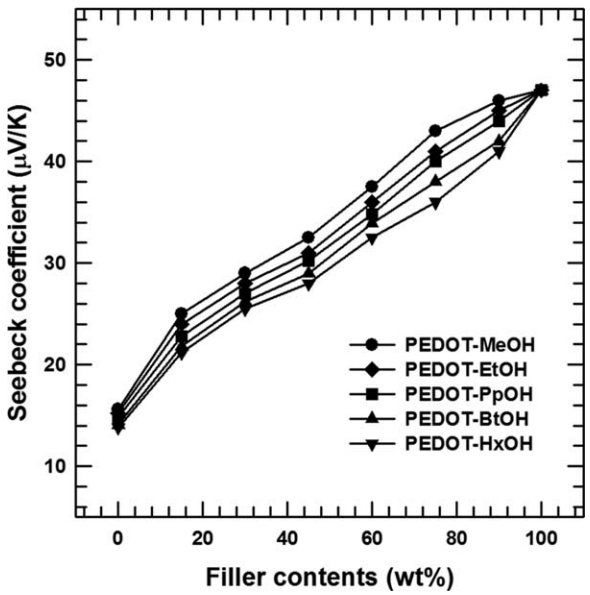

Figure 10. The filler content versus Seebeck coefficient of the PEDOT/graphene composites for PEDOT-MeOH, PEDOT-EtOH, PEDOT-PpOH, PEDOT-BtOH, and PEDOT-HxOH.

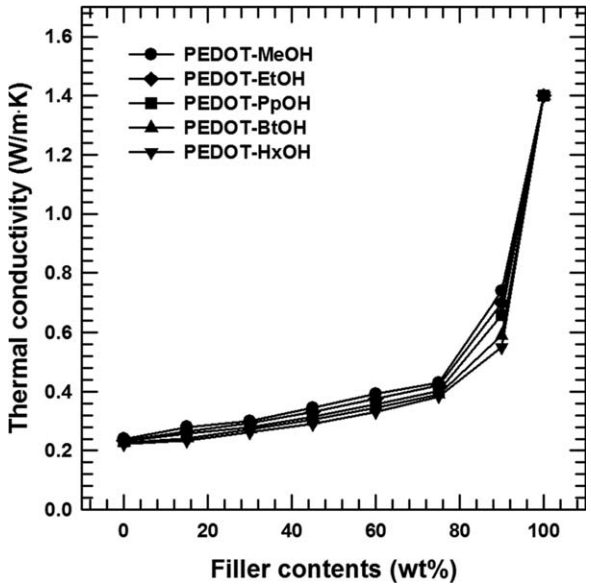

Figure 11. Thermal conductivity of PEDOT/graphene composites for PEDOT-MeOH, PEDOT-EtOH, PEDOT-PpOH, PEDOT-BtOH, and PEDOT-HxOH filled with varied concentrations of graphene.

Seebeck coefficient of the composites, the thermal conductivity was found to be insensitive to the addition of graphene fillers, which exhibited less than only 0.74 W/m K at the filler content of 90 wt %. The thermal conductivity of the TE material is composed of an electronic term from the charge carriers, κ_e, and a lattice term from the phonons, κ_l ($\kappa = \kappa_e + \kappa_l$). The electronic contribution, κ_e can be estimated from the Wiedemann–Franz law:[1–3,26,27]

$$\kappa_e = L \cdot T \cdot \sigma \quad (3)$$

where L is the Lorentz number ($L = 2.45 \times 10^{-8}$ W Ω/K^2). The electronic thermal conductivity (κ_e) changed from only 0.0003 to 0.14 W/m K because the electrical conductivity is low (σ = 0.5–195 S/cm). The small contribution from the electronic term (only about 0.2–23% for the samples) thus entails that the total thermal conductivity mainly depends on the lattice term κ_l. The interfaces between the insulating PEDOT layer and the graphene particles acted as effective phonon scattering centers, which hindered thermal transport due both to the thermally insulating PEDOT barrier and to the graphene acting as impurities in the PEDOT matrix.[8]

Finally, the TE performance of the composites can be evaluated by both the power factor ($S^2\ \sigma$) and the TE figure of merit ($S^2\ \sigma\ T/\kappa$). In Figure 12(a), the power factor increased sharply with increasing graphene filler content, regardless of the solvent. The ZT values of the PEDOT/graphene composites initially increase until reaching a maximum value for the sample with a graphene content of 75 wt % (PEDOT-MeOH, PEDOT-EtOH, and PEDOT-PpOH), and then they decrease dramatically as the graphene content increases. However, the PEDOT-BtOH/graphene composites show a maximum ZT value with a graphene content of 90 wt %. The PEDOT-HxOH/graphene composites show a low efficiency than pristine graphene filler. This different trend is because PEDOT-MeOH, PEDOT-EtOH, and PEDOT-PpOH exhibited high electrical conductivity than PEDOT-BtOH and PEDOT-HxOH, even though the five kinds of PEDOT/graphene composites have similar Seebeck coefficient and thermal conductivity values (PEDOT-MeOH > PEDOT-EtOH > PEDOT-PpOH > PEDOT-BtOH > PEDOT-HxOH). As shown in Figure 12(b), the PEDOT-MeOH with 75 wt % graphene composite had a maximum ZT of 1.9 $\times$ 10^{-2}, higher than that of the other composite materials.

The PEDOT/graphene composites studied in this work showed improved TE performance via a simultaneous increase in both electrical conductivity and Seebeck coefficient, resulting from the increase in carrier mobility. This was attributed to the decrease in the charge carrier hopping barrier via the reduction of intra- and interchain stacking distance caused by a shorter-chain alcoholic

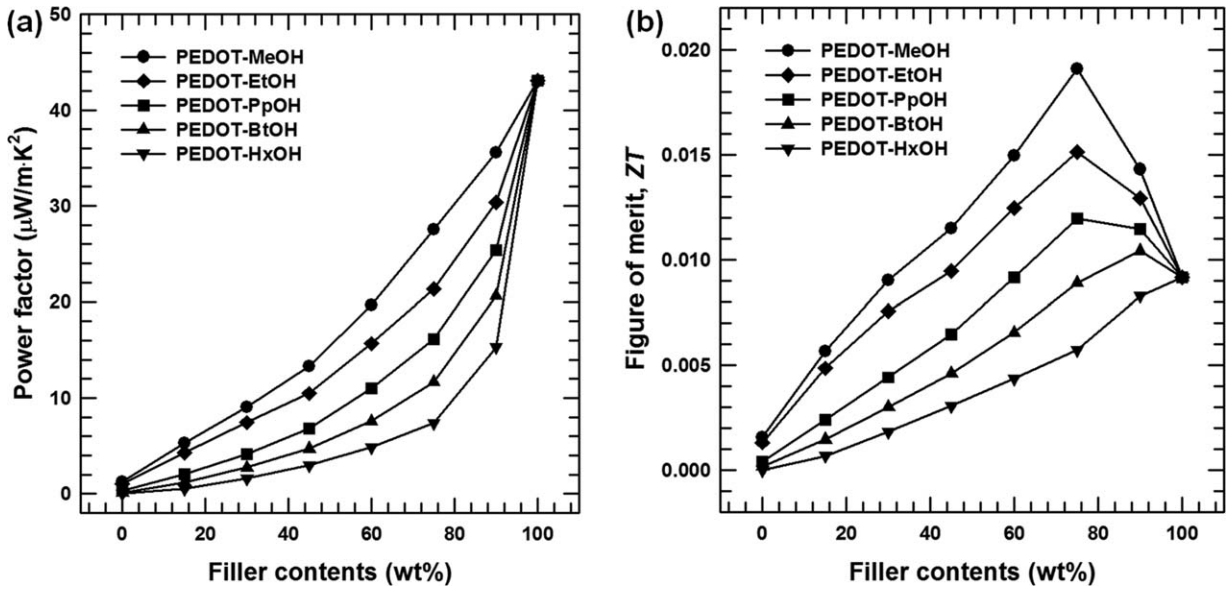

Figure 12. (a) Power factor and (b) figure of merit (ZT) of the PEDOT/graphene composites with graphene content from 0 to 100 wt %.

solvent. Moreover, the graphene filler can develop a strong electrically conductive network with the PEDOT chains, and as a result the charge carrier mobility is increased.

CONCLUSION

TE PEDOT/graphene composites were fabricated in five different types of solvents (methanol, ethanol, 1-propanol, *n*-butanol, and 1-hexanol). $Fe(Bzs)_3$ was chemically synthesized and used as oxidant in the EDOT polymerization process. Before the composite fabrication, DBSA was employed both as surfactant for formation of graphene micelles and as doping agent to coat PEDOT on the graphene surface. Individual graphene fillers were well dispersed into the PEDOT matrix in the synthetic process of the composite, because the coated PEDOT nanolayer had a marked affinity for the PEDOT matrix. XPS analysis showed a 21.7% doping level of the conjugated chain of the PEDOT coating on the graphene surface. TGA results indicated that the graphene filler contained 16.8 wt % of PEDOT coating. PEDOT-MeOH had the highest electrical conductivity among the PEDOT materials. The charge carrier concentration did not contribute to the increase in electrical conductivity, because all PEDOT materials prepared in different alcoholic solvents showed almost the same doping level in the XPS analysis. The main factor in this context was the change of charge carrier mobility: in fact, according to the XRD analysis, the shorter-chain alcoholic solvents enhanced stacking of the PEDOT-Bzs chains, due to the formation of hydrogen bonds between solvent OH groups and sulfonate groups of the benzenesulfonate anion. The decrease of both intra- and interchain stacking distances of the conjugated polymer thus reduced the charge carrier hopping barrier, and as a result the carrier mobility and electrical conductivity were increased. The electrical conductivity of the PEDOT/graphene composite was significantly improved with increasing the graphene filler content. The graphene filler and the conjugated PEDOT chain can form a strong electrically conductive network that increases electron delocalization, and the extended chain conformation reduces the charge carrier hopping barrier, increasing carrier mobility. The Seebeck coefficient of the composites was also enhanced with increasing graphene content, which strongly dependent on the increase of carrier mobility. The thermal conductivity of the composite exhibited relatively small changes, which was attributed to the effect of phonon scattering at the interfaces between graphene and thermally insulating PEDOT layers. This is an ideal result for the improvement of TE properties, because the electrical conductivity and the Seebeck coefficient can be enhanced simultaneously without significant increase in the thermal conductivity. Finally, the maximum ZT of the PEDOT-MeOH/graphene composite with 75 wt % graphene filler content at room temperature exhibited a markedly improved value of 1.9×10^{-2}, higher than that of other PEDOT/graphene composites. The use of shorter-chain alcoholic solvents in the PEDOT synthesis with addition of graphene filler to fabricate TE composites is thus an efficient and promising method to enhance TE properties.

ACKNOWLEDGMENTS

This research was supported by the Chung-Ang University Excellent Student Scholarship in 2014 and Mid-career Researcher Program through NRF grant funded by the MEST(2014R1A2A1A11049625).

REFERENCES

1. Bubnova, O.; Crispin, X. *Energy Environ. Sci.* **2012**, *5*, 9345.
2. Poudel, B.; Hao, Q.; Ma, Y.; Lan, Y.; Minnich, A.; Yu, B.; Yan, X.; Wang, D.; Muto, A.; Vashaee, D.; Chen, X.; Liu, J.; Dresselhaus, M. S.; Chen, G.; Ren, Z. *Science* **2008**, *320*, 634.
3. Kang, J.; Roh, J. W.; Shim, W.; Ham, J.; Noh, J. S.; Lee, W. *Adv. Mater.* **2011**, *23*, 3414.
4. Wang, Q.; Yao, Q.; Chang, J.; Chen, L. *J. Mater. Chem.* **2012**, *22*, 17612.
5. Du, Y.; Cai, K. F.; Shen, S. Z.; Yang, W. D.; Casey, P. S. *J. Mater. Sci.: Mater. Electron.* **2013**, *24*, 1702.
6. Wang, L.; Yao, Q.; Bi, H.; Huang, F. Q.; Wang, Q.; Chen, L. *J. Mater. Chem. A* **2014**, *2*, 11107.
7. Mateeva, N.; Niculescu, H.; Schlenoff, J.; Testardi, L. R. *J. Appl. Phys.* **1998**, *83*, 3111.
8. Kim, G.; Hwang, D.; Woo, S. *Phys. Chem. Chem. Phys.* **2012**, *14*, 3530.
9. Wang, J.; Cai, K.; Shen, S.; Yin, J. *Synth. Met.* **2014**, *195*, 132.
10. Nardes, A. M.; Janssen, R. A.; Kemerink, M. *Adv. Funct. Mater.* **2008**, *18*, 865.
11. Kim, J. Y.; Jung, J. H.; Lee, D. E.; Joo, J. *Synth. Met.* **2002**, *126*, 311.
12. Kim, M.; Yoo, J.; Im, H.; Kim, J. *J. Power Sources* **2013**, *230*, 1.
13. Kim, M.; Hwang, Y.; Kim, J. *Chem. Eng. J.* **2013**, *230*, 482.
14. Zhang, J.; Yang, H.; Shen, G.; Cheng, P.; Zhang, J.; Guo, S. *Chem. Commun.* **2010**, *46*, 1112.
15. Im, H.; Kim, J. *Carbon* **2012**, *50*, 5429.
16. Szymanski, H. IR: Theory and Practice of Infrared Spectroscopy; Plenum Press: New York, **1964**.
17. Seo, K. I.; Chung, I. J. *Polymer* **2000**, *41*, 4491.
18. Han, M. G.; Foulger, S. H. *Adv. Mater.* **2004**, *16*, 231.
19. Zotti, G.; Zecchin, S.; Schiavon, G.; Louwet, F.; Groenendaal, L.; Crispin, X.; Osikowicz, W.; Salaneck, W.; Fahlman, M. *Macromolecules* **2003**, *36*, 3337.
20. Dilks, A. Electron Spectroscopy: Theory, Techniques, and Applications; Brundle, C. R., Baker, A. D., Eds.; Academic Press: London, **1981**.
21. Wang, T.; Qi, Y.; Xu, J.; Hu, X.; Chen, P. *Appl. Surf. Sci.* **2005**, *250*, 188.
22. Ikkala, O. T.; Pietilä, L. O.; Ahjopalo, L.; Österholm, H.; Passiniemi, P. J. *J. Chem. Phys.* **1995**, *103*, 9855.
23. Yao, Q.; Chen, L.; Zhang, W.; Liufu, S.; Chen, X. *ACS Nano* **2010**, *4*, 2445.
24. Hiroshige, Y.; Ookawa, M.; Toshima, N. *Synth. Met.* **2006**, *156*, 1341.
25. Xu, K.; Chen, G.; Qiu, D. *J. Mater. Chem. A* **2013**, *1*, 12395.
26. Meng, C.; Liu, C.; Fan, S. *Adv. Mater.* **2010**, *22*, 535.
27. Im, H.; Kim, J. *Carbon* **2011**, *49*, 3503.